Characterization of Aggregate Received Power from Power Beacons in Millimeter Wave Ad Hoc Networks

Xiaohui Zhou, Salman Durrani and Jing Guo
Research School of Engineering, The Australian National University, Canberra, ACT 2601, Australia.
Emails: {xiaohui.zhou, salman.durrani, jing.guo}@anu.edu.au.

***Abstract*—Wireless power transfer (WPT) has emerged as an attractive solution to power future wireless communication networks. In this paper, we consider WPT using power beacons (PBs) for a millimeter wave (mmWave) wireless ad hoc network. Using stochastic geometry, we derive the moment generating function (MGF) and the nth cumulant of the aggregate received power from PBs at a reference receiver in closed-form. The MGF allows the complementary cumulative distribution function (CCDF) of the aggregate received power from PBs to be numerically evaluated. We also compare different closed-form distributions which can be used to approximate the CCDF of the aggregate received power. Our results show that the lognormal distribution provides the best CCDF approximation compared to other distributions considered in the literature. The results also show that under practical setups, it is feasible to power users in a mmWave ad hoc network using PBs.**

I. Introduction

Wireless power transfer (WPT) is regarded as an attractive solution for future wireless networks [1]. Compared to energy harvesting from the ambient environment (e.g., using solar or ambient radio frequency (RF) energy harvesting), it has the advantage of being always available and controllable. There are currently two major approaches to WPT: (i) simultaneous information and power transfer (SWIPT) where information and power are extracted from the same transmitted signal [1] and (ii) power beacon (PB) based approach where dedicated low-cost transmitters, which do not require backhaul links like normal base stations, are deployed to charge users in their vicinity [2]. In this paper, we adopt the PB based approach in millimeter wave (mmWave) ad hoc networks.

MmWave transmission is a key enabler for future fifth generation (5G) wireless networks, since larger bandwidths are available at mmWave frequencies ($>$ 6 GHz) compared to conventional microwave frequencies ($<$ 6 GHz). MmWave systems have the following two distinctive features which have been recently characterized very well both experimentally [3] and analytically using stochastic geometry [4–7]: (i) propagation environment is more susceptible to blockage causing differences in the line of sight (LOS) and non light of sight (NLOS) path-loss and fading characteristics and the signal to drop out after a certain range and (ii) use of larger antenna arrays (possible due to smaller wavelength) for beamforming at the transmitter and receiver (RX). MmWave transmission is potentially a good combination with WPT, since both technologies operate over short distances and narrow beams in mmWave systems can focus the transmitted power [8].

In WPT systems, the aggregate received power (which determines the harvested power) plays a key role in the system performance. For instance, (i) in SWIPT systems, a common assumption is that the energy constrained node has a large battery to store the received power and, therefore, it transmits with a constant transmit power which is proportional to the aggregate received power [9, 10], (ii) in PB systems, the complementary cumulative distribution function (CCDF) of the aggregate received power plays a key role in determining the power outage probability [2, 11, 12], and (iii) in low power applications, statistical information such as the mean and variance of the aggregate received power can potentially be used to develop efficient sleep and transmission protocols [1, 13]. Thus, it is crucial to accurately characterize the aggregate received power. In this regard, the moment generating function (MGF) of the aggregate received power, which opens the door for application of powerful toolsets from stochastic geometry, has been numerically evaluated in microwave cellular and device-to-device networks with ambient RF energy harvesting [14, 15], mmWave SWIPT systems [6, 7] and microwave PB systems [11]. To the best of our knowledge, a closed-form expression for the MGF of the aggregate received power in mmWave PB systems, incorporating the key propagation characteristics of mmWave transmission, is not available in the literature.

In this paper, we consider a mmWave wireless ad hoc network where PBs are deployed. Using stochastic geometry, we characterize the aggregate received power at a reference RX. The novel contributions of this paper are:

- We derive the closed-form expressions for the MGF and the nth cumulant of the aggregate received power at the reference RX, taking a mmWave three-state propagation model and multi-slope path-loss model into account. The MGF allows the CCDF of the aggregate received power from PBs to be numerically evaluated.
- We test the accuracy of well known closed-form distributions to model the aggregate received power. Our results show that the lognormal distribution provides the best CCDF approximation, compared to other distributions

This work was supported in part by the Australian Research Council's Discovery Project funding scheme (project number DP140101133).

978-1-4673-8999-0/17/$31.00 ©2017 IEEE

commonly considered in the literature.

- We investigate the feasibility of PBs to power users in a mmWave ad hoc network. Our results show that under practical setups, for PB deployment density between $10 - 100$ per km^2, the required PB transmitted power to achieve an average harvested power of 15 dBm is between $1.5-40$ W, which is practical and safe for human exposure.

II. System model

We consider a two-dimensional mmWave wireless ad hoc network, where PBs are deployed to charge users. The PBs are located outdoors and their locations form a homogeneous Poisson point process (PPP) ϕ with density λ. Throughout the paper, we use X_i to denote both the random location as well as the ith PB itself. The PBs have access to a dedicated power supply (e.g., a battery or power grid) and transmit with constant power P using beamforming. The PB transmissions set up an energy field over the wireless ad hoc network region and users harvest power from the aggregate PB received signal [16]. We assume that the PBs randomly and independently choose a direction to point their main beams. Given a sufficient density of the PBs, this simple strategy ensures that the aggregate received power from PBs at different locations in the network is roughly on the same order. Similarly, the users point their main beam in a randomly chosen direction. This avoids the need for channel estimation and accurate beam alignment. In this paper, without loss of generality, we focus on the characterization of the aggregate received power from PBs at an outdoor reference RX, Y_0, located at the origin.

MmWave Blockage Model: For outdoor mmWave transmissions, each link between the ith PB and the reference RX is susceptible to building blockages due to their high diffraction and penetration characteristics [4]. In this work, we adopt the state-of-the-art three-state blockage model [5], where each link can be in one of the following three states: (i) the link is in LOS state if no blockage exists, (ii) the link is in NLOS state if blockage exists and (iii) the link is in outage (OUT) state if the link is too weak to be established.

Assuming that the link between the ith PB and the RX has a Euclidean length of $r_i = \|X_i - Y_0\|$, the probabilities $p_{\mathrm{LOS}}(\cdot)$, $p_{\mathrm{NLOS}}(\cdot)$ and $p_{\mathrm{OUT}}(\cdot)$ of it being in LOS, NLOS and OUT states, respectively, are

$$\begin{aligned} p_{\mathrm{OUT}}(r_i) &= u(r_i - r_{\max}); \\ p_{\mathrm{NLOS}}(r_i) &= u(r_i - r_{\min}) - u(r_i - r_{\max}); \\ p_{\mathrm{LOS}}(r_i) &= 1 - u(r_i - r_{\min}), \end{aligned} \tag{1}$$

where $u(\cdot)$ denotes the unit step function, $r_{\min}$ is the radius of the LOS region and $r_{\max}$ is the exclusion radius of the OUT region. The values of $r_{\min}$ and $r_{\max}$ depend on the propagation scenario and the carrier frequency. Typical values used in this work are summarized in Table II.

MmWave Channel Model: Measurements have shown that mmWave links experience different channel conditions under LOS, NLOS and OUT states [3]. Hence, in this work, we adopt a path-loss plus fading channel model as follows.

We assume that a link in LOS state experiences Nakagami-m fading, while a link in NLOS state experiences Rayleigh fading. For the path-loss, we modify and adapt a multi-slope path-loss model and define the path-loss between the ith PB and the reference RX with a distance of r_i as follows

$$l(r_i) = \begin{cases} 1, & 0 \leqslant r_i < 1 \\ r_i^{-\alpha_{\mathrm{L}}}, & 1 \leqslant r_i < r_{\min} \\ \beta r_i^{-\alpha_{\mathrm{N}}}, & r_{\min} \leqslant r_i < r_{\max} \\ \infty, & r_{\max} \leqslant r_i \end{cases}, \tag{2}$$

where the first condition is added to ensure a bounded path-loss model, α_{L} denotes the path-loss exponent for the link in LOS state and subscript L denotes LOS, α_{N} denotes the path-loss exponent for the link in NLOS state ($2 \leqslant \alpha_{\mathrm{L}} \leqslant \alpha_{\mathrm{N}}$) and subscript N denotes NLOS, the path-loss of the link in OUT state is assumed to be infinite [5] and the continuity in the multi-slope path-loss model is maintained by introducing the constant $\beta \triangleq r_{\min}^{\alpha_{\mathrm{N}} - \alpha_{\mathrm{L}}}$ [17]. We also define $\delta_{\mathrm{L}} = \frac{2}{\alpha_{\mathrm{L}}}$ and $\delta_{\mathrm{N}} = \frac{2}{\alpha_{\mathrm{N}}}$ for convenience in presenting the analytical results in Section III.

Beamforming Model: We assume that antenna arrays are used for beamforming at both the PBs and the reference RX. Following [4, 5], we approximate the actual antenna array pattern by a sectorized gain pattern which can be expressed as

$$G_a(\theta) = \begin{cases} G_a^{\max}, & |\theta| \leq \frac{\theta_a}{2} \\ G_a^{\min}, & \text{otherwise} \end{cases}, \tag{3}$$

where subscript $a = p$ for PB and $a = r$ for reference RX, $G_a^{\max}$ is the main lobe antenna gain, $G_a^{\min}$ is the side lobe antenna gain, $\theta \in [-\pi, \pi)$ is the angle off the boresight direction and θ_a is the main lobe beam-width. Note this model can be easily related to specific array geometries, such as an N element uniform planar or linear or circular array [18].

As stated earlier, the main beam at the PBs and RX are assumed to be randomly oriented with respect to each other and uniformly distributed in $[-\pi, \pi)$. Let G_i be the effective antenna gain on the link from the ith PB to the reference RX. As a result of sectorization, G_i is a discrete random variable with probability distribution as $G_i = G_k$ with probability p_k, $k \in \{1, 2, 3, 4\}$. The values of G_k and p_k are summarized in Table I.

TABLE I
Probability mass function of G_i

k	Gain G_k	Probability p_k
1	$G_p^{\max} G_r^{\max}$	$\frac{\theta_p \theta_r}{4\pi^2}$
2	$G_p^{\max} G_r^{\min}$	$\frac{\theta_p (2\pi - \theta_r)}{4\pi^2}$
3	$G_p^{\min} G_r^{\max}$	$\frac{(2\pi - \theta_p)\theta_r}{4\pi^2}$
4	$G_p^{\min} G_r^{\min}$	$\frac{(2\pi - \theta_p)(2\pi - \theta_r)}{4\pi^2}$

Power Transfer Model: We assume that the reference RX is equipped with a typical rectifier-based power receiver to

harvest power from the aggregate PB received signal [16]. Practical rectifier-based power receivers have a power receiver activation threshold ϵ, i.e., the power receiver is only activated when the aggregate received power from all the PBs is greater than ϵ [11]. We assume that once the power receiver is properly activated, then the harvested power is linearly proportional to the aggregate received power from the PBs and the constant of proportionality η is the power conversion efficiency.

III. Aggregate Received Power from Power Beacons

In this section, we provide the mathematical formulation to characterize the aggregate received power at the reference RX from all PBs.

Since the power harvested from the noise is negligible, the instantaneous aggregate received power at the reference RX from all the PBs can be expressed as

$$P_{\text{agg}} = P \sum_{X_i \in \phi} G_i h_i l(r_i), \tag{4}$$

where P is the PB transmitted power, G_i is the effective antenna gain between X_i and Y_0, h_i is the fading power gain between X_i and Y_0, which follows the gamma distribution (under the Nakagami-m fading assumption) if the link is in LOS state and exponential distribution (under the Rayleigh fading distribution) if the link is in NLOS state and $l(r_i)$ is the path-loss function in (2).

Note that P_{agg} in (4) is a random variable because of the randomness in the antenna gain, mmWave channels and locations of PBs. We use stochastic geometry to find its CCDF and also its nth cumulant.

A. CCDF and MGF of the Aggregate Received Power from Power Beacons

The CCDF of the aggregate received power at the reference RX from all the PBs can be obtained by using the Gil-Pelaez inversion theorem [19]

$$\Pr(P_{\text{agg}} > z) = \frac{1}{2} + \frac{1}{\pi} \int_0^\infty \text{Im}[\mathcal{M}_{P_{\text{agg}}}(-j\omega) \exp(-j\omega z)] \frac{d\omega}{\omega}, \tag{5}$$

where $\Pr(\cdot)$ denotes the probability, $\text{Im}[\cdot]$ denotes the imaginary part of a complex number, $j = \sqrt{-1}$ is the imaginary unit, $\mathcal{M}_{P_{\text{agg}}}(s) = \mathbb{E}[\exp(-sP_{\text{agg}})]$ is the MGF of P_{agg} and $\mathbb{E}[\cdot]$ is the expectation operator.

The following proposition characterizes the exact MGF of P_{agg} in closed-form.

Proposition 1: The MGF of the aggregate received power at the reference RX from all the PBs in a mmWave ad hoc network, following the system model in Section II, is

$$\begin{aligned}\mathcal{M}_{P_{\text{agg}}}(s) = \prod_{k=1}^{4} \exp\Big(&\pi\lambda r_{\text{min}}^2 p_k \big(m^m (m + s r_{\text{min}}^{-\alpha_{\text{L}}} PG_k)^{-m} - 1\big) \\ &+ \pi\lambda p_k \left(sPG_k\right)^{\delta_{\text{L}}} \left(\Xi_1\left(1\right) - \Xi_1\left(r_{\text{min}}\right)\right) \\ &+ \pi\lambda p_k sPG_k\beta \left(\Xi_2(r_{\text{min}}) - \Xi_2(r_{\text{max}})\right) \\ &+ \frac{\pi\lambda}{2+\alpha_{\text{N}}} p_k (sPG_k\beta)^{\delta_{\text{N}}} \left(\Xi_3(r_{\text{min}}) - \Xi_3(r_{\text{max}})\right)\Big),\end{aligned} \tag{6}$$

where

$$\Xi_1(r) = \frac{m^m (r^{-\alpha_{\text{L}}} sPG_k)^{-\delta_{\text{L}}-m} \alpha_{\text{L}} \Gamma(1+m)}{(2+m\alpha_{\text{L}})\Gamma(m)} \times {}_2F_1\left(1+m, m+\delta_{\text{L}}; 1+m+\delta_{\text{L}}; -\frac{m r^{\alpha_{\text{L}}}}{sPG_k}\right), \tag{7}$$

$$\Xi_2(r) = \frac{r^2}{r^{\alpha_{\text{N}}} + sPG_k\beta}, \tag{8}$$

$$\Xi_3(r) = \frac{(r^{-\alpha_{\text{N}}} sPG_k\beta)^{-\delta_{\text{N}}-1}}{r^{\alpha_{\text{N}}} + sPG_k\beta} \Big(sPG_k\beta(2+\alpha_{\text{N}}) - 2(r^{\alpha_{\text{N}}} + sPG_k\beta) {}_2F_1\Big(1, \delta_{\text{N}}+1; 2+\delta_{\text{N}}; -\frac{r^{\alpha_{\text{N}}}\beta^{-1}}{sPG_k}\Big)\Big), \tag{9}$$

where $\Gamma(\cdot)$ is the Gamma function and ${}_2F_1(\cdot,\cdot;\cdot;\cdot)$ is the Gaussian (or ordinary) hypergeometric function.

Proof: See Appendix A. ∎

Remark 1: To the best of our knowledge, Proposition 1 presents the result for the MGF of P_{agg} in closed-form for the first time in the literature In addition, (6) substituted in (5) allows the CCDF to be numerically computed. Note that although the MGF in (6) is in closed-form, the CCDF in (5) cannot be expressed in closed-form due to complexity of the MGF which is inside the integration. However, it can be easily evaluated numerically using Mathematica.

B. nth Cumulant of the Aggregate Received Power from Power Beacons

The nth cumulant of the aggregate received power at the reference RX from all the PBs, $\kappa_{P_{\text{agg}}}(n)$, can also be expressed in terms of the MGF of P_{agg} as [20]

$$\kappa_{P_{\text{agg}}}(n) = (-1)^n \frac{d^n \ln \mathcal{M}_{P_{\text{agg}}}(s)}{ds^n}\Big|_{s=0}, \tag{10}$$

where $\ln$ is the natural logarithm. The following proposition characterizes the nth cumulant of P_{agg} in closed-form.

Proposition 2: The nth cumulant of the aggregate received power at the reference RX from all the PBs in a mmWave ad hoc network, following the system model in Section II, is given by

$$\kappa_{P_{\text{agg}}}(n) = \sum_{k=1}^{4} \left(\Psi_k^1(n) - \Psi_k^2(n) - \Psi_k^3(n)\right), \tag{11}$$

where

$$\Psi_k^1(n) = \pi\lambda p_k P^n G_k^n m^{-n} \frac{\Gamma(m+n)}{\Gamma(m)}, \tag{12}$$

$$\Psi_k^2(n) = \begin{cases} 2\pi\lambda p_k PG_k \ln r_{\text{min}}, & \alpha_{\text{L}}=2 \;\&\; n=1 \\ \frac{2\pi\lambda\Gamma(m+n)\left(1-r_{\text{min}}^{-n\alpha_{\text{L}}+2}\right)}{\Gamma(m)(2-n\alpha_{\text{L}})} p_k \left(\frac{PG_k}{m}\right)^n, & \text{otherwise} \end{cases}, \tag{13}$$

$$\Psi_k^3(n) = \frac{2\pi\lambda\left(r_{\text{min}}^{-n\alpha_{\text{N}}+2} - r_{\text{max}}^{-n\alpha_{\text{N}}+2}\right)}{2-n\alpha_{\text{N}}} p_k P^n G_k^n \beta^n \Gamma(1+n). \tag{14}$$

Proof: See Appendix B. ∎

C. Closed-form Approximation of the CCDF of the Aggregate Received Power

Since the exact CCDF of the aggregate received power cannot be expressed in closed-form, we test various distributions which can be used to approximate the CCDF in this section. The distribution of P_{agg} is approximated by the well known closed-form distributions by second-order moment matching, i.e., by matching the mean and the variance of the two distributions, where the mean and the variance of P_{agg} can be found from Proposition 2. First, we present the skewness and the kurtosis of P_{agg}, which are two important measures of a real-valued random variable.

Skewness and Kurtosis of P_{agg}: The skewness and the kurtosis describe the shape of the probability distribution of P_{agg} and are given by

$$\text{Skew}\left[P_{\text{agg}}\right] = \frac{\kappa_{P_{\text{agg}}}(3)}{\kappa_{P_{\text{agg}}}(2)^{1.5}}, \tag{15}$$

$$\text{Kurt}\left[P_{\text{agg}}\right] = \frac{\kappa_{P_{\text{agg}}}(4)}{\kappa_{P_{\text{agg}}}(2)^{2}}. \tag{16}$$

The skewness shows whether a distribution is left or right tailed and the kurtosis measures the heaviness of the tail.

Gaussian Distribution: The CCDF of the Gaussian distribution is

$$\Pr\left(P_{\text{agg}} > z\right)^{\text{Gaussian}} = Q\left(\frac{z - \kappa_{P_{\text{agg}}}(1)}{\sqrt{\kappa_{P_{\text{agg}}}(2)}}\right), \tag{17}$$

where $Q(\cdot)$ is the Q-function, $\kappa_{P_{\text{agg}}}(1)$ and $\kappa_{P_{\text{agg}}}(2)$ are the first and the second cumulant of P_{agg}, respectively, which can be calculated by (11).

Lognormal Distribution: The CCDF of the lognormal distribution is

$$\Pr\left(P_{\text{agg}} > z\right)^{\text{lognormal}} = Q\left(\frac{\ln z - \mu^{\text{lognormal}}}{\sigma^{\text{lognormal}}}\right), \tag{18}$$

where $\mu^{\text{lognormal}}$ and $\sigma^{\text{lognormal}}$ are the location parameter and the scale parameter given by

$$\mu^{\text{lognormal}} = \ln\left(\frac{\kappa_{P_{\text{agg}}}(1)}{\sqrt{1 + \frac{\kappa_{P_{\text{agg}}}(2)}{\kappa_{P_{\text{agg}}}(1)^2}}}\right), \tag{19}$$

$$\sigma^{\text{lognormal}} = \sqrt{\ln\left(1 + \frac{\kappa_{P_{\text{agg}}}(2)}{\kappa_{P_{\text{agg}}}(1)^2}\right)}. \tag{20}$$

Gamma Distribution: The CCDF of the Gamma distribution is

$$\Pr\left(P_{\text{agg}} > z\right)^{\text{gamma}} = 1 - \frac{\gamma\left(k^{\text{gamma}}, \frac{z}{\theta^{\text{gamma}}}\right)}{\Gamma\left(k^{\text{gamma}}\right)}, \tag{21}$$

where $\gamma(\cdot,\cdot)$ is the lower incomplete gamma function, $k^{\text{gamma}} = \frac{\kappa_{P_{\text{agg}}}(1)^2}{\kappa_{P_{\text{agg}}}(2)}$ and $\theta^{\text{gamma}} = \frac{\kappa_{P_{\text{agg}}}(2)}{\kappa_{P_{\text{agg}}}(1)}$ are the shape parameter and scale parameter of gamma distribution, respectively.

TABLE II
SIMULATION PARAMETERS

Notation	Parameter	Value
α_{L}	LOS link path-loss exponent	$\{2, 2.5\}$
α_{N}	NLOS link path-loss exponent	4
P	PB transmitted power	10 dB
λ	density of PB PPP	$10^5 \sim 1$ per km^2
r_{min}	radius of the LOS region	$\{50$ m, 100 m$\}$
r_{max}	exclusion radius of the OUT region	200 m
m	Nakagami-m fading parameter	$\{5, 10\}$
$f_{h_{\text{L}}}(h)$	LOS link channel fading PDF	$\frac{m^m h^{m-1} \exp(-mh)}{\Gamma(m)}$
$f_{h_{\text{N}}}(h)$	NLOS link channel fading PDF	$\exp(-h)$
G_p^{max}, G_p^{min}, θ_p	PB beamforming parameter	$\{[0$ dB, 0 dB, $360^{\text{o}}]$, $[20$ dB, -10 dB, $30^{\text{o}}]$, $[30$ dB, -10 dB, $6^{\text{o}}]\}$
G_r^{max}, G_r^{min}, θ_r	RX beamforming parameter	$\{[0$ dB, 0 dB, $360^{\text{o}}]$, $[10$ dB, -10 dB, $45^{\text{o}}]\}$
η	power conversion efficiency	0.5

IV. RESULTS

In this section, we present the analytical or numerical results and compare with the simulation results. The simulation results are generated by averaging over 10^8 Monte carlo simulation runs. The values of the main parameters are summarized in Table II, which are chosen to be consistent with the literature in mmWave and WPT [1, 4]. Note that if the distance between the PB and the RX is more than $r_{\text{max}} = 200$ m, the mmWave link is in OUT state.

A. Distribution Approximation of the Aggregate Received Power

The skewness and the kurtosis of P_{agg} versus the density of PB λ are plotted in Fig. 1(a) and 1(b) respectively for different path-loss exponents of LOS link $\alpha_{\text{L}} = 2, 2.5$ and different Nakagami-m fading parameters $m = 5, 10$. We can see that the curves are monotonic for the considered range of λ. Smaller α_{L} and larger m lead to smaller skewness and kurtosis. As the density of PB increases, the gap between the different curves becomes smaller. The distribution of the aggregate received power is skewed to the right with a heavy tail, because both the skewness and the kurtosis of P_{agg} are much greater than 0. Moreover, the skewness and the kurtosis of a Gaussian distributed random variable are 0. Hence, we can conclude that the aggregate received power under the considered system model does not converge to a Gaussian distribution (even for the very extreme case with a PB density of 0.1 per m^2).

Fig. 1(c) plots the exact and approximated CCDF of P_{agg} for $\alpha_{\text{L}} = 2$ and $m = 5$. The simulation results assume the LOS links undergo Rician fading with $K = 10$ dB. The exact CCDF is plotted numerically using (5) and (6), while the approximated CCDFs are obtained using (17) for Gaussian distribution, (18) for lognormal distribution and (21) for gamma distribution. From the figure, we can see that the CCDF of P_{agg} under Rician fading LOS links can be closely approximated by Nakagami-m fading by adjusting the m values. Gaussian distribution does not provide a good approximation, which agrees with our discussion above. Gamma distribution is found

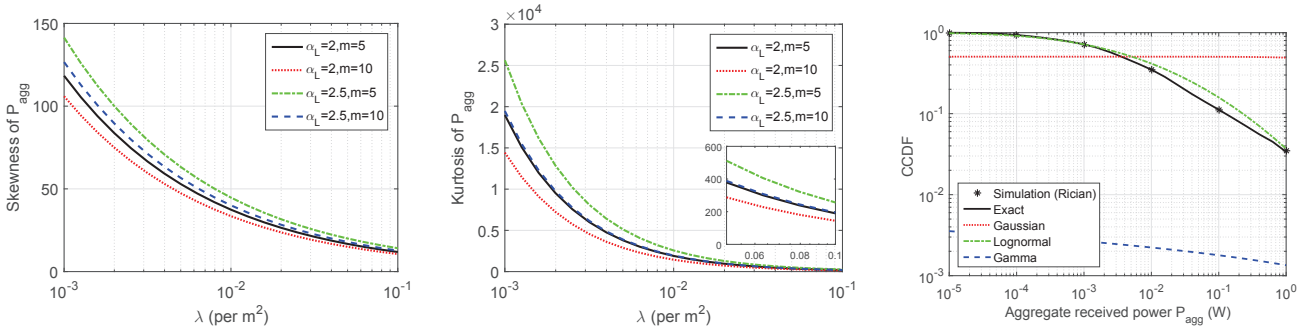

(a) Skewness of the aggregate received power versus the density of PB for different path-loss exponents and Nakagami-m fading parameters for LOS links.

(b) Kurtosis of the aggregate received power versus the density of PB for different path-loss exponents and Nakagami-m fading parameters for LOS links.

(c) CCDF approximation of the aggregate received power P_{agg} of networks in which LOS links experience Nakagami-m fading with $m = 5$ and simulation of networks in which LOS links experience Rician fading with $K = 10$ dB. The PB density is 10^{-4} per m^2 and the path-loss exponent of LOS links is 2.

Fig. 1. Skewness, kurtosis and CCDF approximation of the aggregate received power with the radius of the LOS region being 100 m and the PB and RX beamforming parameter being [20 dB, -10 dB, 30°] and [10 dB, -10 dB, 45°] respectively.

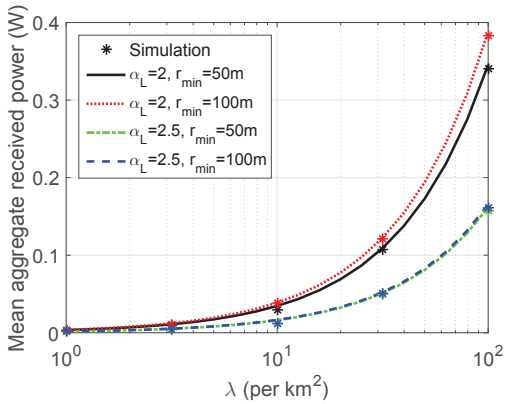

Fig. 2. Mean aggregate received power versus the density of PB for different path-loss exponents of LOS links and different radius of the LOS region with the Nakagami-m fading parameter being 5 and the PB and RX beamforming parameter being [20 dB, -10 dB, 30°] and [10 dB, -10 dB, 45°] respectively.

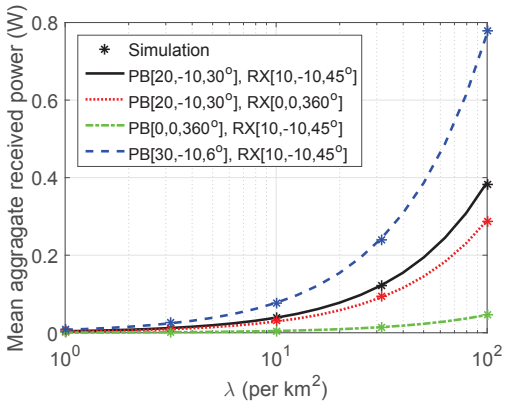

Fig. 3. Mean aggregate received power versus the density of PB for different beamforming parameters for PB and RX with the radius of the LOS region being 100 m and the path-loss exponent being 2 and the Nakagami-m fading parameter being 5 for LOS links.

to provide a close approximation to the power distribution of homogeneous PPP network [21] and heterogeneous PPP network [22] with non-singular path-loss model, but it clearly does not provide a good fit under the mmWave system model. We have tested the CCDF approximations using inverse Gaussian distribution, exponential distribution, Suzuki distribution and inverse gamma distribution against the exact CCDF and Rician LOS fading simulation under different channel parameters as well. However, they perform poorly and the results are omitted here for the sake of brevity. Overall, our results show that lognormal distribution provides the best CCDF approximation of P_{agg}.

B. Mean Aggregate Received Power

Next, we investigate the impact of the channel parameters and the beamforming parameters on the the mean aggregate received power $\overline{P_{\text{agg}}} = \kappa_{P_{\text{agg}}}(1)$.

Fig. 2 plots $\overline{P_{\text{agg}}}$ against the density of PB for different path-loss exponents of LOS link $\alpha_{\text{L}} = 2, 2.5$ and different radius of the LOS region $r_{\text{min}} = 50$ m, 100 m. We can see that the simulation results match perfectly with the analytical results. The figure also shows that $\overline{P_{\text{agg}}}$ increases with λ. With smaller α_{L} and larger r_{min}, $\overline{P_{\text{agg}}}$ grows at a faster rate. When $\alpha_{\text{L}} = 2.5$, the traces of two different r_{min} overlap. We can see that the benefit of increasing the radius of the LOS region is insignificant, when α_{L} is large.

Fig. 3 plots $\overline{P_{\text{agg}}}$ against the density of PB for different beamforming parameter for PB $[0$ dB$, 0$ dB$, 360°]$, $[20$ dB$, -10$ dB$, 30°]$, $[30$ dB$, -10$ dB$, 6°]$ and TX $[0$ dB$, 0$ dB$, 360°]$, $[10$ dB$, -10$ dB$, 45°]$. Again the simulation results match perfectly with the analytical results. We can see that a narrower main lobe beam-width gives a larger main lobe gain which results in a faster rate of growth of $\overline{P_{\text{agg}}}$ with

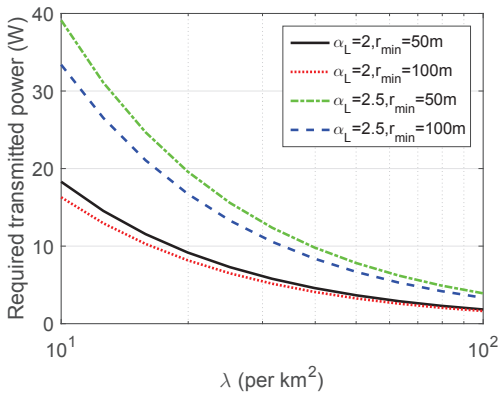

Fig. 4. Required transmitted power of PB versus the density of PB for different path-loss exponents of LOS links and different radius of the LOS region with the Nakagami-m fading parameter being 5 and the PB and RX beamforming parameter being [20 dB, -10 dB, 30°] and [10 dB, -10 dB, 45°] respectively.

respect to λ.

C. Feasibility of WPT via PBs

In this section, we examine the feasibility of WPT via PBs in a mmWave ad hoc network. In this regard, it is important to note that the electronic circuitry of a power receiver has an activation threshold which has a value typically between -30 dBm and -20 dBm [1]. In addition, the typical maintenance power for a smart phone is between 20 mW and 30 mW [23].

Fig. 4 plots the required transmitted power of PB to achieve an average harvested power of 15 dBm ($= 31.62$ mW), which is the typical maintenance power for a smart phone and is much higher than the power sensitivity level, versus the density of PB by assuming a constant power conversion efficiency of $\eta = 0.5$. From the figure, we can see that for a fixed PB density the decrease in the LOS path-loss exponents brings a higher saving in the transmitted power needed than the increase in the radius of LOS region. From Fig. 4, the maximum transmitted power required at a PB density of 10 per km^2 is 39.12 W. If PB transmits with this maximum value, the power density at a distant of 1 m from the PB is 3.113 W/m^2. This power density is smaller than 10 W/m^2, which is the permissible safety level of human exposure to RF electromagnetic fields based on IEEE Standard [16].

V. Conclusions

In this paper, the mmWave wireless ad hoc network where RX harvests energy from all PBs was considered. We first derived the MGF and the nth cumulant of the aggregate received power at the RX to study the CCDF of the aggregate received power. Furthermore, we compared the different closed-form distributions which can be used to approximate the characteristics of the aggregate received power. Our results showed that the lognormal distribution provided the best CCDF approximation compared to other distributions considered in the literature for microwave network. The results have also shown that application of mmWave PB is feasible under practical network setup.

Appendix A
Proof of Proposition 1

Following the definition of MGF,

$$\mathcal{M}_{P_{\text{agg}}}(s) = \mathbb{E}\left[\exp(-sP_{\text{agg}})\right] = \mathbb{E}[\exp(-sP\sum_{X_i\in\phi} G_i h_i l(r_i))]$$
$$= \mathbb{E}[\exp(-sP\sum_{0\leqslant r_i<1} G_i h_i l(r_i))]$$
$$\times\, \mathbb{E}[\exp(-sP\sum_{1\leqslant r_i<r_{\min}} G_i h_i l(r_i))]$$
$$\times\, \mathbb{E}[\exp(-sP\sum_{r_{\min}\leqslant r_i<r_{\max}} G_i h_i l(r_i))]$$
$$= \underbrace{\exp\left(-\int_{-\pi}^{\pi}\int_{0}^{1}\mathbb{E}_{h_i,G_i}[1-\exp(-sPG_ih_i)]\lambda r dr d\theta\right)}_{A_1}$$
$$\times\underbrace{\exp\left(-\int_{-\pi}^{\pi}\int_{1}^{r_{\min}}\mathbb{E}_{h_i,G_i}[1-\exp(-sPG_ih_i r^{-\alpha_{\text{L}}})]\lambda r dr d\theta\right)}_{A_2}$$
$$\times\underbrace{\exp\left(-\int_{-\pi}^{\pi}\int_{r_{\min}}^{r_{\max}}\mathbb{E}_{h_i,G_i}[1-\exp(-sPG_ih_i\beta r^{-\alpha_{\text{N}}})]\lambda r dr d\theta\right)}_{A_3}, \quad (22)$$

where $\mathbb{E}_{h_i,G_i}$ represents the expectation with respect to h_i and G_i. The first term A_1 is evaluated as follows.

$$A_1 = \exp\left(-\pi\lambda\left(1-\mathbb{E}_{h_i,G_i}\left[\exp(-sPG_ih_i)\right]\right)\right)$$
$$= \exp\left(-\pi\lambda + \pi\lambda m^m \mathbb{E}_{G_i}\left[\left(m+sr_{\min}^{-\alpha_{\text{L}}}PG_i\right)^{-m}\right]\right)$$
$$= \exp\left(-\pi\lambda + \pi\lambda m^m \sum_{k=1}^{4}\left(m+sr_{\min}^{-\alpha_{\text{L}}}PG_k\right)^{-m}p_k\right), \quad (23)$$

where we use the fact that the link in LOS state experiences Nakagami-m fading with $f_{h_{\text{L}}}(h) = \frac{m^m h^{m-1}\exp(-mh)}{\Gamma(m)}$.

The second term A_2 is evaluated as follows.

$$A_2 = \exp\Big(\pi\lambda\mathbb{E}_{h_i,G_i}\left[1-\exp(-sPG_ih_i)\right]$$
$$-\pi\lambda r_{\min}^2\mathbb{E}_{h_i,G_i}\left[1-\exp(-sr_{\min}^{-\alpha_{\text{L}}}PG_ih_i)\right]$$
$$-\pi\lambda\mathbb{E}_{h_i,G_i}\left[(sPG_i)^{\delta_{\text{L}}}h_i^{\delta_{\text{L}}}\gamma(1-\delta_{\text{L}},sPh_iG_i)\right]$$
$$+\pi\lambda\mathbb{E}_{h_i,G_i}\left[(sPG_i)^{\delta_{\text{L}}}h_i^{\delta_{\text{L}}}\gamma(1-\delta_{\text{L}},sPh_iG_ir_{\min}^{-\alpha_{\text{L}}})\right]\Big) \quad (24a)$$
$$= \exp\Bigg(\pi\lambda-\pi\lambda m^m\sum_{k=1}^{4}\left(m+sPG_k\right)^{-m}p_k-\pi\lambda r_{\min}^2$$
$$+\sum_{k=1}^{4}\pi\lambda r_{\min}^2 m^m\left(m+sr_{\min}^{-\alpha_{\text{L}}}PG_k\right)^{-m}p_k$$
$$-\pi\lambda\sum_{k=1}^{4}(sPG_k)^{\delta_{\text{L}}}\frac{m^m(sPG_k)^{-\delta_{\text{L}}-m}\alpha_{\text{L}}\Gamma(1+m)}{(2+m\alpha_{\text{L}})\Gamma(m)}$$
$$\times\ {}_2F_1\left(1+m,m+\delta_{\text{L}};1+m+\delta_{\text{L}};-\frac{m}{sPG_k}\right)p_k$$
$$+\pi\lambda\sum_{k=1}^{4}(sPG_k)^{\delta_{\text{L}}}\frac{m^m(r_{\min}^{-\alpha_{\text{L}}}sPG_k)^{-\delta_{\text{L}}-m}\alpha_{\text{L}}\Gamma(1+m)}{(2+m\alpha_{\text{L}})\Gamma(m)}$$
$$\times\ {}_2F_1\left(1+m,m+\delta_{\text{L}};1+m+\delta_{\text{L}};-\frac{r_{\min}^{\alpha_{\text{L}}}m}{sPG_k}\right)p_k\Bigg), \quad (24b)$$

where (24a) follows from changing variables and integration by parts and (24b) is obtained after taking the expectation over h_{L} then G_i.

Similarly, the third term A_3 can be worked out by taking the expectation over h_{N}, which has a PDF as $f_{h_{\mathrm{N}}}(h) = \exp(-h)$. The details are omitted for sake of brevity. Finally, the MGF expression in Proposition 1 is obtained by substituting $A1$, $A2$ and $A3$ into (22).

Appendix B
Proof of Proposition 2

We cannot obtain the nth cumulant of P_{agg} by directly substituting (6) into (10), as the cumulant becomes incomputable at $s = 0$. Instead, we use the integration form of the MGF in (22) and substitute in (10) to obtain

$$\kappa_{P_{\text{agg}}}(n) = (-1)^{n+1}\Bigg(\underbrace{\frac{d^n}{ds^n}\int_{-\pi}^{\pi}\int_{0}^{1}\mathbb{E}_{h_i,G_i}[1-\exp(-sPG_ih_i)]\lambda r dr d\theta\Big|_{s=0}}_{B_1}$$
$$+\underbrace{\frac{d^n}{ds^n}\int_{-\pi}^{\pi}\int_{1}^{r_{\min}}\mathbb{E}_{h_i,G_i}[1-\exp(-sPG_ih_ir^{-\alpha_{\mathrm{L}}})]\lambda r dr d\theta\Big|_{s=0}}_{B_2}$$
$$+\underbrace{\frac{d^n}{ds^n}\int_{-\pi}^{\pi}\int_{r_{\min}}^{r_{\max}}\mathbb{E}_{h_i,G_i}[1-\exp(-sPG_ih_i\beta r^{-\alpha_{\mathrm{N}}})]\lambda r dr d\theta\Big|_{s=0}}_{B_3}\Bigg), \quad (25)$$

where . The first term B_1 is evaluated as follows.

$$\begin{aligned}B_1 &= \int_{-\pi}^{\pi}\int_{0}^{1}\mathbb{E}_{h_i,G_i}\left[\frac{d^n 1-\exp(-sPG_ih_i)}{ds^n}\Big|_{s=0}\right]\lambda r dr d\theta\\ &= \int_{-\pi}^{\pi}\int_{0}^{1}\mathbb{E}_{h_i,G_i}\left[(-1)^{n+1}(PG_ih_i)^n\right]\lambda r dr d\theta\\ &= (-1)^{n+1}P^n\pi\lambda\mathbb{E}_{h_i}\left[h_i^n\right]\mathbb{E}_{G_i}\left[G_i^n\right]\\ &= (-1)^{n+1}P^n\pi\lambda m^{-n}\frac{\Gamma(m+n)}{\Gamma(m)}\sum_{k=1}^{4}G_k^n p_k. \end{aligned} \quad (26)$$

Similarly, the terms B_2 and B_3 can be derived by following similar steps as above. Substituting B_1, B_2 and B_3 into (25) gives the nth cumulant expression in Proposition 2.

References

[1] X. Lu, P. Wang, D. Niyato, D. I. Kim, and Z. Han, "Wireless networks with RF energy harvesting: A contemporary survey," *IEEE Commun. Surveys Tuts.*, vol. 17, no. 2, pp. 757–789, Second-quarter 2015.

[2] K. Huang and V. K. N. Lau, "Enabling wireless power transfer in cellular networks: Architecture, modeling and deployment," *IEEE Trans. Wireless Commun.*, vol. 13, no. 2, pp. 902–912, Feb. 2014.

[3] M. R. Akdeniz, Y. Liu, M. K. Samimi, S. Sun, S. Rangan, T. S. Rappaport, and E. Erkip, "Millimeter wave channel modeling and cellular capacity evaluation," *IEEE J. Sel. Areas Commun.*, vol. 32, no. 6, pp. 1164–1179, June 2014.

[4] J. G. Andrews, T. Bai, M. N. Kulkarni, A. Alkhateeb, A. K. Gupta, and R. W. Heath, "Modeling and analyzing millimeter wave cellular systems," *IEEE Trans. Commun.*, vol. 65, no. 1, pp. 403–430, Jan. 2017.

[5] M. D. Renzo, "Stochastic geometry modeling and analysis of multi-tier millimeter wave cellular networks," *IEEE Trans. Wireless Commun.*, vol. 14, no. 9, pp. 5038–5057, Sep. 2015.

[6] T. A. Khan, A. Alkhateeb, and R. W. Heath, "Millimeter wave energy harvesting," *IEEE Trans. Wireless Commun.*, vol. 15, no. 9, pp. 6048–6062, Sep. 2016.

[7] L. Wang, M. Elkashlan, R. W. Heath, M. D. Renzo, and K. K. Wong, "Millimeter wave power transfer and information transmission," in *Proc. IEEE GLOBECOM*, Dec. 2015.

[8] A. Ghazanfari, H. Tabassum, and E. Hossain, "Ambient RF energy harvesting in ultra-dense small cell networks: performance and trade-offs," *IEEE Wireless Commun.*, vol. 23, no. 2, pp. 38–45, Apr. 2016.

[9] Y. Deng, L. Wang, M. Elkashlan, M. D. Renzo, and J. Yuan, "Modeling and analysis of wireless power transfer in heterogeneous cellular networks," *IEEE Trans. Commun.*, vol. 64, no. 12, pp. 5290–5303, Dec. 2016.

[10] S. Akbar, Y. Deng, A. Nallanathan, M. Elkashlan, and A. H. Aghvami, "Simultaneous wireless information and power transfer in k-tier heterogeneous cellular networks," *IEEE Trans. Wireless Commun.*, vol. 15, no. 8, pp. 5804–5818, Aug. 2016.

[11] J. Guo, S. Durrani, X. Zhou, and H. Yanikomeroglu, "Outage probability of ad hoc networks with wireless information and power transfer," *IEEE Wireless Commun. Lett.*, vol. 4, no. 4, pp. 409–412, Aug. 2015.

[12] D. Oliveira and R. Oliveira, "Characterization of energy availability in RF energy harvesting networks," *Math. Probl. Eng.*, vol. 2016, pp. 1–9, 2016.

[13] W. Liu, X. Zhou, S. Durrani, H. Mehrpouyan, and S. D. Blostein, "Energy harvesting wireless sensor networks: Delay analysis considering energy costs of sensing and transmission," *IEEE Trans. Wireless Commun.*, vol. 15, no. 7, pp. 4635–4650, July 2016.

[14] A. H. Sakr and E. Hossain, "Cognitive and energy harvesting-based D2D communication in cellular networks: Stochastic geometry modeling and analysis," *IEEE Trans. Wireless Commun.*, vol. 63, no. 5, pp. 1867–1880, May 2015.

[15] ——, "Analysis of k-tier uplink cellular networks with ambient RF energy harvesting," *IEEE J. Sel. Areas Commun.*, vol. 33, no. 10, pp. 2226–2238, Oct. 2015.

[16] M. Xia and S. Aissa, "On the efficiency of far-field wireless power transfer," *IEEE Trans. Signal Process.*, vol. 63, no. 11, pp. 2835–2847, June 2015.

[17] X. Zhang and J. G. Andrews, "Downlink cellular network analysis with multi-slope path loss models," *IEEE Trans. Commun.*, vol. 63, no. 5, pp. 1881–1894, May 2015.

[18] K. Venugopal, M. C. Valenti, and R. W. Heath, "Device-to-device millimeter wave communications: Interference, coverage, rate, and finite topologies," *IEEE Trans. Wireless Commun.*, vol. 15, no. 9, pp. 6175–6188, Sep. 2016.

[19] M. D. Renzo and P. Guan, "Stochastic geometry modeling of coverage and rate of cellular networks using the Gil-Pelaez inversion theorem," *IEEE Commun. Lett.*, vol. 18, no. 9, pp. 1575–1578, Sep. 2014.

[20] A. Papoulis and S. U. Pillai, *Probability, Random Variables and Stochastic Processes*, 4th ed. McGraw-Hill, 2002.

[21] R. K. Ganti and M. Haenggi, "Interference in ad hoc networks with general motion-invariant node distributions," in *Proc. IEEE ISIT*, July 2008.

[22] R. W. Heath, M. Kountouris, and T. Bai, "Modeling heterogeneous network interference using poisson point processes," *IEEE Trans. Signal Process.*, vol. 61, no. 16, pp. 4114–4126, Aug. 2013.

[23] H. Xia, B. Natarajan, and C. Liu, "Feasibility of simultaneous information and energy transfer in LTE-A small cell networks," in *Proc. IEEE CCNC*, Jan. 2014.